Ph.D. Thesis

In vitro and *in silico* investigation of degradation of CAD/CAM resin composites by water absorption

Osaka University Graduate School of Dentistry

Course for Oral Sciences

Chunwoo Lee

Table of contents

I. Introduction

Computer-aided design/computer-aided manufacturing (CAD/CAM) systems have been widely used in dentistry [1-3] since the first dental CAD/CAM restoration was introduced in the 1980s [4, 5]. Among CAD/CAM materials, CAD/CAM resin composites have promising clinical performance [6, 7], esthetic appearance [8], uniform quality [9], and machinability [6, 10]. CAD/CAM resin composites consist of a matrix resin and inorganic fillers treated with a saline coupling agent [11-13]. The matrix resin forms the basis of the composite structure and comprises organized methacrylate-derived polymers such as urethane dimethacrylate (UDMA), bisphenol A-glycidyl methacrylate (Bis-GMA), or triethylene glycol dimethacrylate (TEGDMA) [12]. Inorganic fillers, commonly made of silica, zirconia, and alumina, can be used to reinforce the composite structure because of their high mechanical properties [14-16]. For CAD/CAM resin composites, 0.1 μm or smaller nano-fillers of chemically stable inorganic materials are often used to improve the mechanical properties and provide polishability for a smooth surface [17-21]. Because inorganic fillers are chemically stable, a surface modification using silane coupling agents is required to adhere the fillers to an organic matrix resin [22-24]. Gamma-methacryloyloxypropyl trimethoxysilane (γ-MPTS) is a typical silane

coupling agent that forms a 1.9–3.0 nm thick layer between fillers and the matrix resin [25, 26]. CAD/CAM resin composites are manufactured with the components described above under high temperature and high-pressure polymerization to enhance the mechanical properties via an increase in density and degree of crosslinking [21, 27].

However, resin composites are susceptible to degradation by water absorption. Since the matrix resin is an ester form derived from methacrylate [28, 29], degradation of the methacrylate group via hydrolysis of the ester bonds occurs when water is absorbed [30, 31]. Additionally, water ingress leads to hydrolytic breakdown of the bond between the silane and filler particles [32, 33]. This water-induced degradation negatively impacts the restoration longevity and mechanical properties [11, 32-35]. While these degradations have been reported qualitatively, quantitative details have not yet been revealed, especially in silane coupling layers, because arbitral control of the silane coupling ratio of the filler is not possible with conventional *in vitro* tests.

Rigorous mathematical theories of homogenization have been proposed for quantitative analysis of the composite materials [36-38]. These theories assumed that the material properties are periodic functions of the micro-scale variables, where the period is very small compared with the macro-scale variables. With this assumption, equivalent material properties in the macro-scale dimension can be calculated from known or arbitral

micro-scale properties. This approach was recently applied to the analysis of more complex structured materials, including micro-structured materials, such as porous ceramics [39] and titanium [40], and also nano-structured polymer composites [41-44] *in silico*. In dentistry, *in silico* homogenization analysis has been used to investigate multifactorial issues such as the effect of the nano-filler particle diameter on the physical properties of CAD/CAM resin composites [45], the effect of different designs and materials of the endocrown on the stress distribution and failure probability [46], and the influence of resorption cavities on the mechanical properties and load distribution in cortical bone after implant placement [47].

A modeling procedure of *in silico* homogenization analysis is required for its practical use. Digital image-based modeling is employed because the procedure for a complex three-dimensional structure of heterogeneous materials, such as composite materials, is burdensome. The first proposal was attempted in the biomechanical area to model the porous microstructure of human bone [48, 49]. Applications for digital imaging by a flat-bed scanner or micro computed tomography (CT) were reported for the study of concrete [50], porous ceramic [39], titanium [40], and composite materials [51]. Furthermore, modeling by cryo-electron microscopy has been introduced to capture a nano-scale structure such as a nano-filler composite.

In vitro high-resolution imaging enables the analysis of a nano-scale structure, which produces an accurate model reflecting morphological compositions. *In silico* homogenization allows arbitral control of the properties, which enables identification of the main factor of physio-mechanical issues at the macro-scale. Therefore, the combination of *in vitro* and *in silico* approaches may enable quantitative investigation of the degradation of CAD/CAM resin composites by water absorption.

The aim of this study was to quantitatively evaluate how water absorption of the CAD/CAM resin composites affect the matrix resin and silane coupling layer using *in vitro* high-resolution imaging and *in silico* homogenization.

II. Investigation on the influence of water absorption on the bulk block and matrix resin

1. Purpose

The aim of this chapter was to investigate the influence of water absorption on a CAD/CAM resin composite bulk block and an experimental matrix block (EMB) by water immersion. A water sorption test and *in vitro*/*in silico* three-point bending test were conducted. *In silico* homogenization analysis with a simplified model was also conducted to reassess the three-point bending test results.

2. Materials and methods

1) Materials used

Katana Avencia P block (Kuraray Noritake Dental, Tokyo, Japan; KAP) and EMB (Kuraray Noritake Dental) were used (Table 1). EMB was made only of a matrix resin that consisted of urethane dimethacrylate (UDMA) and triethylene glycol dimethacrylate (TEGDMA), and was manufactured at the same temperature and pressure as KAP, excluding fillers (Figure 1).

2) Water sorption test

A water sorption test was conducted to confirm the water-absorbing property of KAP and EMB. The test was conducted according to ISO 4049:2019 [52]. Disk shaped specimens of KAP and EMB (ϕ 14 × 1 mm) were fabricated. The specimens (n = 10 for each material) were alternately dried at 37°C for 22 hours and 22°C for 2 hours in a vacuum chamber until the weight converged as required in the ISO 4049:2019 drying protocol. After the initial dry, the specimens were immersed in distilled water for seven days at 37°C. The specimens were then dried again by the step described above. The water sorption (W_{sp}) value was determined by Formula (1):

$$W_{sp}\ (\mu g/mm^3) = \frac{M_1 - M_2}{V} \quad (1)$$

where M_1 is the weight of the specimen after immersion (μg), M_2 is the weight of the specimen after re-dry (μg), and V is the volume of the specimen (mm^3).

3) Three-point bending test

A three-point bending test was conducted to evaluate the reduction of the elastic modulus before and after immersion for KAP and EMB. The blocks were sliced with a low speed precision cutter (IsoMet, Buehler, Illinois, USA) to 14 × 4.0 × 1.2 mm according to Japan Dental Materials Association Standards (JDMAS) 245:2017 specifications. Ten specimens were left untreated as the before-immersion group, and another ten specimens were stored in distilled water for seven days at 37°C as the after-immersion group. A three-point bending test was conducted using a universal testing machine (EZ-SX, Shimadzu, Kyoto, Japan). The maximum load was 500 N and the crosshead speed was 1 mm/min. The *in vitro* load–displacement curves were obtained and the flexural strain (δ) was calculated by Formula (2):

$$\delta = \frac{6Dd}{L^2} \quad (2)$$

where D is the maximum deflection of the center of the beam (mm), d is the thickness of the tested beam (mm), and L is the support span (mm).

The flexural strains of the before- and after-immersion groups were analyzed by a Student's *t*-test with a level of statistical significance of $\alpha = 0.05$ using statistical analysis software (IBM SPSS Statistics 24, IBM, New York, USA).

The *in silico* non-linear finite element analysis (NLFEA) method was employed for evaluating the elastic modulus of the materials. The three-point bending test environment was simulated with NLFEA software (LS-DYNA, Ansys, Pennsylvania, USA). The simulation parameters were flexural strain, density, and arbitral elastic modulus. The flexural strain was taken from the result of the *in vitro* three-point bending test. The density was calculated directly by dividing the weight of the specimen measured using a precision digital weighing scale (GR-120, A&D, Tokyo, Japan) with the volume of the specimen estimated by micro-CT (R_mCT2, Rigaku, Tokyo, Japan). An *in silico* three-point bending analysis was repeatedly conducted by changing the elastic modulus. When the root mean squared error of load in the *in vitro* and *in silico* load–displacement curve was less than 1 N, the arbitral elastic modulus was determined as a true elastic modulus of the material (Figure 2).

4) *In silico* homogenization analysis

In silico homogenization analysis was used to determine whether the factor for degrading the elastic modulus of the bulk block was the matrix resin or not. For this test, the *in silico* model of KAP (KAP model) was composed in a voxel-based FEA

software (VOXELCON2015, Quint, Tokyo, Japan). The parameters were based on reported values: the filler size was 38.6 nm, the elastic modulus of the filler was 70 GPa, and the thickness of the silane coupling layer was 2 nm [21, 25, 26, 53]. The elastic modulus of the matrix resin area was set according to the result of the three-point bending test of EMB. The properties and shape of the KAP model are shown in Table 2 and Figure 3. The elastic moduli of the KAP model were calculated as before- and after-immersion according to the elastic modulus of EMB in the corresponding condition. The elastic moduli of the model were compared with the KAP result to determine whether the elastic modulus was reduced by water immersion.

3. Results

1) Value for water absorption

The water absorption values for KAP and EMB were 0.0183 μg/mm^3 and 0.0363 μg/mm^3, respectively.

2) Elastic modulus and flexural strain

The load–displacement curves of the *in vitro* and *in silico* three-point bending tests

are shown in Figure 4. The elastic modulus of KAP was 13 GPa in the before-immersion group, and was 12 GPa in the after-immersion group. During water immersion, the elastic modulus decreased by 1 GPa over seven days of water immersion. The elastic modulus of the EMB decreased 0.3 GPa over the same time, from 3 GPa in the before-immersion group to 2.7 GPa in the after-immersion group. The flexural strain of KAP was 0.024±0.0024 in the before-immersion group, and was 0.025±0.0027 in the after-immersion group. The flexural strain of EMB was 0.12±0.022 in the before-immersion group, and was 0.12 ± 0.012 in the after-immersion group. For both KAP and EMB, the flexural strain before and after water immersion was not significantly different ($p > 0.05$).

3) Elastic modulus in the *in silico* model

The *in silico* analysis employing the KAP model showed an inconsistent trend in the reduction of the elastic modulus with water immersion with the KAP block. The elastic modulus of the KAP model in the before-immersion condition was the same as the KAP block of 13 GPa and the elastic modulus of the KAP model in the after-immersion condition was 12.7 GPa.

4. Summary

KAP and EMB showed a water-absorbing feature and the elastic moduli of both blocks decreased with water absorption. Since EMB was manufactured in the same scheme as the matrix resin area of KAP, one of the reasons to induce performance deterioration of the CAD/CAM resin composites by water absorption was degradation of the matrix resin. However, *in silico* homogenization analysis showed that the elastic modulus change of the KAP model was less than that of the KAP block. As a result, the matrix resin and other factors contribute to reducing the elastic modulus of CAD/CAM resin composites.

III. Verification of the physicochemical change of the silane coupling layer by water immersion

1. Purpose

In this chapter, the morphological change of the surface of the CAD/CAM resin composites after water immersion was observed by scanning probe microscopy (SPM). The increase in the number of hydroxyl groups in the silane coupling layer with water immersion was evaluated by X-ray photoelectron spectroscopy (XPS). In addition, the relationship between the silane coupling ratio and elastic modulus of the CAD/CAM resin composites was investigated by an *in silico* homogenization method to verify how the degradation of the silane coupling layer affected the bulk block.

2. Materials and methods

1) Material used

The Katana Avencia block (Kuraray Noritake Dental; KAB) was used. The composition of the KAB is shown in Table 3.

2) Nano-scale observation of the surface morphological change

For nano-scale observation by SPM, two specimen bars from the KAB (7.0 × 4.0 × 1.2 mm) were sliced with a low speed precision cutter (IsoMet). The specimens were then polished using #1000 and #2000 SiC paper, followed by #4000 alumina-containing abrasive emulsion. One specimen was used a control without treatment, and the other specimen was immersed in distilled water for seven days at 37°C. The specimens were observed by a scanning probe microscope (SPM-9700HT, Shimadzu) using the lateral force microscopy (LFM) mode. The observed surface areas of the specimen were 500 × 500 nm. The generated surface friction signals were stored as 256 × 256 pixel images, where the pixels of a high friction signal area were an indicator of the degraded region.

3) Investigation of the amount of hydrolysis of the silane coupling layer

Hydrolysis is a chemical reaction in which a molecule of water ruptures the chemical bonds, producing a hydroxyl group. Therefore, focusing on the hydroxyl group is a reasonable method to evaluate the hydrolysis. XPS and a chemical labeling technique were used to evaluate the amount of hydroxyl groups [54-56]. Fluoride was used because of its sensitivity to XPS. The binding energy of the electron in 1s orbital of Fluoride (F1s) was observed to confirm changes in the hydroxyl group.

A KAB block was sliced to a size of 7.0 × 4.0 × 1.2 mm with a low speed precision cutter (IsoMet). Five specimens were allocated to the before-immersion group (control, no treatment) and after-immersion group where the specimens were immersed in distilled water for seven days at 37°C. The specimens of both groups were subject to a decontamination process by boiling in a 5 w/w% sodium peroxodisulfate ($N_2O_2O_8$) solution for 15 minutes, followed by ultrasonic rinsing with 70% ethanol. 1H,1H,2H,2H-perfluorooctyldimethylchlorosilane ($C_{10}H_{10}ClF_{13}Si$, FUJIFILM Wako chemicals, Osaka, Japan; PFODMCS) was used for fluoride labeling (Figure 5). Specimens were treated with a 5% PFODMCS solution in 99% ethanol for two hours at 60°C. The effectiveness of the fluoride-labeling process was determined by energy-dispersive X-ray spectroscopy (EDX). An XPS (JPS-9010, JEOL, Tokyo, Japan) investigation was used to evaluate the amount of fluoride with the atomic percentage of the F1s.

The atomic percentage of F1s in the before- and after-immersion specimens were analyzed by a Student's *t*-test with a level of statistical significance of $\alpha = 0.05$ using a statistical analysis software (IBM SPSS Statistics 24).

4) *In silico* homogenization analysis

The nanoscale CAD/CAM resin composite model was designed with 3D CAD software (SolidWorks 2011, Dassault Systèmes SolidWorks, Vélizy-Villacoublay, France). In a matrix cube of 90 nm, 12 spherical fillers with a diameter of 40 nm were placed regularly (Figure 6). The thickness of the silane coupling layer was defined as 2 nm, which ensured the minimum thickness of a voxel (1 nm) and reflected the theoretical silane chain length [57]. The elastic moduli of the components and volume ratios are shown in Table 4. To simulate different silane coupling ratios, seven different layers of 0-elastic modulus that represent uncoupled layers were arranged (Table 5, Figure 7). The nanoscale model and uncoupled layers were combined, and the elastic moduli were calculated by homogenization analysis in voxel-based FEA software (VOXELCON2015).

3. Results

1) Nano-scale surface morphology change

Figure 8 shows the nano-scale surface morphology of the specimens observed by SPM. The degraded areas are represented as a black region (black arrows). There was more degraded area in the after-immersion group than the before-immersion group.

The filler outline was clearly observed in Figure 8b and not in Figure 8a.

2) Amount of hydrolysis of the silane coupling layer

To verify the amount of hydrolysis, PFODMCS was used to label the hydroxyl groups in the CAD/CAM resin composites as a fluoride marker and EDX was performed. As shown in Figure 9, pale yellow dots represent the fluoride atom location. Since the fluoride atoms were settled near the fillers where the silane coupling agent was covered, the labeling process was successfully achieved.

The XPS F1s peak at 692 eV representing PFODMCS attached to the hydroxyl group is shown in Figure 10. The atomic percentage of F1s in the after-immersion group was 14.31%, which was significantly greater than that in the before-immersion group (11.52%), suggesting that the hydrolysis of the silane coupling layer occurred during water immersion (Figure 11).

3) Silane coupling ratio and corresponding elastic modulus

The silane coupling ratios and corresponding elastic moduli from *in silico* homogenization analysis are shown in Table 6. The elastic modulus of the bulk model non-linearly decreased as the silane coupling ratio decreased.

4. Summary

The SPM investigation revealed more degraded area in the specimen of the after-immersion group than the before-immersion group. Since the only difference in condition was the immersion, the water immersion degraded the matrix resin and the silane coupling layer. Moreover, the F1s peak in the XPS spectra and the greater atomic percentage in the after-immersion group than the before-immersion group suggests that hydrolysis in the silane coupling layer proceeded during water immersion.

In silico homogenization analysis showed that a decrease in the elastic modulus occurred in conjunction with a decrease in the silane coupling ratio. When this result is combined with the SPM and XPS results, it can be deduced that water immersion may cause reduction of the elastic modulus of the bulk block by impairment of the silane coupling layer as well as the matrix resin.

IV. Prediction of the amount of degradation of the silane coupling layer in CAD/CAM resin composite blocks

1. Purpose

This chapter was used to build CAD/CAM resin composite models that reflected the shape of the filler. The amount of hydrolysis of the silane coupling layer by water absorption was calculated with the resulting model.

2. Materials and methods

1) Materials used

The Katana Avencia block (Kuraray Noritake Dental; KAB) described in Chapter III and the experimental matrix block (EMB) described in Chapter II were used.

2) Three-point bending test

A three-point bending test was conducted to evaluate the reduction of the elastic modulus before and after immersion for KAB and EMB. The specimen preparation and evaluation of the elastic moduli were conducted as described in Chapter II.

3) Reconstruction of the nano-scale model to reflect the filler shape

Images of KAB were acquired using scanning electron microscopy/focused ion beam (Quanta™ 3D FEG, FEI, Eindhoven, The Netherlands) with a cryo preparation system (PP-3000T, Quorum Technology, East Sussex, United Kingdom) at semi-cryogenic temperature of −130°C. The inspection region was 1.8 × 1.4 × 1.2 μm, and 213 images were obtained. The pixel resolution was 2.9 nm and the slice thickness was 5.8 nm. These images were saved in an uncompressed tagged image file format (TIFF) as an image stack (Figure 12).

The saved image stack was pre-processed to enhance the filler margin, to reduce noise, and remove artifacts by image process software (ImageJ, National Institute of Health, Bethesda, Maryland, USA). The fillers and matrix resin in the images were separated by setting a threshold for binarization. The threshold value was defined such that the volume ratio of fillers satisfied the product specification of KAB. Then, each filler in the binary-colored images were segmented using the Watershed algorithm because the fillers were aggregated for the xy-plane, yz-plane, and zx-plane. Sharp edges of the segmented fillers were smoothed using the Remove Outliers algorithm to produce naturally rounded edges (Figure 13). The pre-processed image stack was saved as topography of the fillers.

A three-dimensional model of KAB was reconstructed in voxel-based FEA software (VOXELCON2015) by importing the topography of the fillers into a rectangular volume of the matrix (Figure 14). Five sub-models of a 100 nm cube were extracted randomly from the original three-dimensional model for calculation because of computational power limitations, and the silane space was applied around the fillers using a Dilate algorithm (Figure 15).

4) Prediction of the coupling ratio

Eleven coupling ratios (100, 95, 90, 85, 80, 75, 70, 65, 60, 55, 50%) of the silane coupling layer and the corresponding elastic moduli were calculated with the voxel-based FEA software (VOXELCON2015).

To determine the coupling ratio, *in silico* homogenization analysis was conducted with sub-models of a 100 nm cube in three steps. First, the elastic modulus of a sub-model (EM_{model}) was calculated with elastic modulus of the matrix (EM_{matrix}), filler (EM_{filler}), and arbitral elastic modulus of the silane coupling layer ($arbEM_{silane}$) in the voxel-based FEA software. Second, if EM_{model} and the elastic modulus of (EM_{block}) were the same, $arbEM_{silane}$ was considered a true elastic modulus of the silane coupling layer (EM_{silane}) and proceeded to the third sequence. Otherwise, $arbEM_{silane}$ was

updated and the first step was repeated. Third, the coupling ratio was determined with EM_{silane} using the elastic modulus and coupling ratio of the silane coupling layer relation described above.

3. Results

1) Elastic modulus

The load–displacement curves of the *in vitro* and *in silico* three-point bending tests are shown in Figure 16. The elastic modulus of KAB was 8.2 GPa and 6.9 GPa for the before- and after-immersion groups, respectively. The elastic modulus of EMB is referred to in Chapter II (Table 7).

2) Nano-scale model

The generated sub-models had irregularly shaped fillers. Within the sub-models, the volume ratio of the filler was 55.12 ± 0.271%. The elastic modulus was 11.01 ± 0.345 GPa when the silane coupling was assumed to be fully accomplished.

3) Predicted coupling ratio

The coupling ratios and corresponding elastic moduli of the silane coupling layers

are summarized in Table 8. The unknown coupling ratio for a particular elastic modulus was interpolated using the relation between the coupling ratio and elastic modulus. Using repetitive calculation, the elastic modulus of the silane coupling layer was determined to be 1.16 ± 0.05 GPa for the before-immersion condition. For this elastic modulus, the coupling ratio was predicted to be 78.2 ± 1.64%. For the after-immersion condition, the elastic modulus of the silane coupling layer was determined to be 0.92 ± 0.04 GPa, corresponding to 68.4 ± 0.89% of the coupling ratio (Table 9).

4. Summary

A model of the CAD/CAM resin composites reflecting the nano-filler shape was successfully developed using cryo-electron microscopy, which was not possible by conventional imaging techniques. *In silico* homogenization analysis revealed that the elastic modulus of the CAD/CAM resin composites under 100% silane coupled conditions was 11.01 GPa, while the elastic modulus of KAB of the before-immersion group was 8.2 GPa. These results suggest that 100% silane coupling in KAB was not obtained in the manufacturing process. Additionally, the silane coupling ratio of KAB decreased by 9.8% after seven days of water immersion.

V. Discussion

This study was performed to clarify how water absorption of the CAD/CAM resin composites quantitatively affect the matrix resin and silane coupling layer, especially the reduction of the silane coupling ratio. The silane coupling layer is a critical component to the CAD/CAM resin composites because it determines the physio–mechanical properties. Since CAD/CAM resin composites are materials typically used in humid conditions, quantitative clarification of the change in those conditions is important. Previous studies have qualitatively revealed the degradation aspect of the CAD/CAM resin composites by water absorption. However, the quantitative details have not been fully revealed, especially regarding the silane coupling layer, because of experimental limitations of nano-scale manipulation. Thus, an attempt at combining an *in vitro* high-resolution technique and *in silico* homogenization analysis was used to demonstrate the intact silane coupling ratio.

In Chapter II, KAP showed a water-absorbing feature, suggesting water is incorporated into the matrix resin. Water absorption is described by a dual-mode theory, which considers that absorbed water molecules have two natures [58]. One is held by ordinary molecular dissolution in the matrix resin and the other is physically trapped in polymer

micro-voids. The absorbed water is molecularly dispersed into the matrix resin and acts as a plasticizer, causing swelling of the polymer. The quantity of this absorbed water depends on the equilibrium volume, physicochemical affinity to the polymer, and the resistance of polymer chains to swelling deformation stress. This water serves as a proton donor and causes chemical reaction with the matrix resin or silane coupling agents. Alternatively, the water molecules that are accommodated in micro-voids are formed of hydrogen bonds, acting as filler particles. These water molecules increase the elastic modulus of the bulk block after water absorption [59, 60]. In this study, water molecules function as a proton donor rather than as a filler, reducing the elastic modulus.

For cured UDMA, which is the main matrix resin materials of KAP, the time to reach sorption is six days [61]. Since the duration of water immersion was seven days in this experiment, water was considered to be sufficiently incorporated into the matrix resin. Water uptake into the CAD/CAM resin composites causes extraction of the unreacted components and the degradation process, including hydrolysis of the components contacting water molecules [62]. For the matrix resin, hydrolysis occurs at the resin ester bonds, resulting in degradation of the matrix resin and release of the degradation products [30]. Even KAP is manufactured at a high temperature and pressure to suppress voids and unreacted monomers, the polymerization process is never complete and unreacted

monomers can remain in the composites [63]. Thus, the matrix resin of KAP is not robust to water.

The *in silico* analysis of Chapter II indicates factors other than the matrix resin can reduce the elastic modulus of the bulk block by water absorption. For instance, degradation of the silane coupling layers is considered an important factor. Water molecules likely enter silane-treated layers and gradually hydrolyze siloxane bonding between fillers and water molecules, hydrating the resultant hydroxysilyl group [24, 64, 65]. There are several approaches to improve the coupling ability using novel silane coupling agents and silanation processes. The hydrolytic instability of the silane coupling agent is still complicated, reducing the flexural properties [66].

The model used in Chapter II was assumed to have spherical fillers. Although the filler shape of KAP is described as a spherical nanofiller according to the manufacturer's specification, the geometry of the fillers was verified as a clustered irregular shape by SEM. A limitation of this *in silico* homogenization analysis in Chapter II was that the filler shape was spherical, which is not fully reflected even if the shapes of the fillers affect the mechanical properties of the bulk block [67]. However, the reduction in the elastic modulus of the condition after immersion was different than that observed from the three-point bending test results.

SPM and XPS are versatile tools for the study of the surface nano-morphology and chemical state [56, 68, 69]. SPM has been used to investigate the nanomechanical characterization of materials [69, 70]. Among the SPM techniques, LFM is used to measure the lateral torsion of the cantilever during scanning motion. Since the torsion reflects the frictional properties of a surface, intact or brittle areas on the sample surface can be detected with nanometer resolution [69, 71]. However, environmental noise and external disturbance are likely to cause probe vibration, which affects the imaging quality [72]. The blurry SPM images of Chapter III are attributed to such probe vibration. However, the intact area, including fillers and degraded area, were distinguishable and the surface properties of the specimens before and after water immersion were observed. There was more degraded area in the after-immersion group than the before-immersion group, whereas the fillers in the after-immersion group were clearer than the before-immersion group because of degradation to the matrix resin and silane coupling layer during water immersion.

The change in XPS F1s atomic percentage showed a change in the amount of hydroxyl groups, which was an indicator of hydrolysis. Although XPS analysis can be used to qualitatively assess the target atom [54, 73, 74], hydroxyl groups developed on the silane coupling layer as well as the surface of the fillers. Therefore, assessing the absolute

amount of the hydrolyzed silane coupling layer was impractical. However, considering the fact that silica filler is chemically stable in water, it can be assumed that the amount of hydroxyl groups on the silica filler was constant. The XPS analysis results can be considered valid even if the absolute amount of hydrolysis cannot be estimated.

The elastic modulus of the 75.5% silane coupling model decreased to 16.8% compared with that of the 100% silane coupling model. This result supports the fact that excessive water uptake may decrease the elastic modulus for resin composites further [13] because of hydrolytic degradation [63]. The decrease in elastic modulus may induce debonding of the CAD/CAM resin composite prosthetics by deformation of the margin [75].

In Chapter IV, the CAD/CAM resin composites were scanned using cryo-electron microscopy to obtain three-dimensional reconstructions. A high-resolution and non-destructive method was required to design a model to thoroughly reflect the size and shape of fillers with a mean size of a few nanometers. The advantages of cryo-electron microscopy are the non-destructive determination of the internal structure from nanometer scale electron density differences [76] compared with micro-CT that only has micro-scale resolution and focused ion beam/SEM that can deform the material [77]. When investigating CAD/CAM resin composites by cryo-electron microscopy, image processing and segmentation algorithms were necessary.

Since all of the mechanical properties of each component in the *in silico* nano-scale model could not be evaluated individually, the general parameters were based on a similar study [45] that was used to determine the elastic modulus of models. In the previous study, the effects of the nano-filler particle diameter on the elastic modulus of the CAD/CAM resin composites were investigated. The results suggest that smaller filler particles increased the elastic modulus. In this study, the elastic moduli of the 100-nm sub-models were not proportional to the filler content. Since the size of the nano-fillers in each sub-model were not constant, the models with smaller fillers resulted in a higher elastic modulus. Additionally, even if the diameter of the fillers are the same, the mechanical properties of the bulk block varies by the filler shape [78-82]. Although a direct comparison between the filler shape and elastic modulus was not conducted in this study, a disproportional trend between the elastic modulus and filler content indicated that the elastic modulus of the bulk block was not related only to the filler content, suggesting a coincidence with the previous study [83].

The coupling ratio of KAB in the before-immersion condition was predicted to be 78.2%, which suggests that silane coupling was not completely achieved even in the manufacturing process. A silane coupling agent consists of an organofunctional group, alkoxy group, and linker group [57]. To adhere inorganic substrates, a alkoxy group

should be activated by acid to form a silanol [24, 84]. This activation process is affected by the bulkiness of the alkoxy group [85], concentration, pH [86], temperature [87], humidity, and solvent system [88].

The reaction between the organofunctional group and matrix resin is induced by the reactive free radicals generated by the initiator in the matrix resin [89]. Since the coupling ratio is affected by the silane agent activation and radical reaction, inactivated alkoxy groups and unreacted free radicals induce the collapse of the coupling ratio. Various efforts have been used to improve the coupling ratio. To enhance activation of the silane coupling agent, the concentration of the silane coupling agent, heat applied during silanation, and pH of the silanation vehicle have been regulated [57, 66]. Surface treatment of the inorganic fillers by pyrochemical coating [90] or hydrofluoric acid treatment [91] have been used to increase the reaction between the filler and silanol group. To improve the bonding between the organofunctional group and matrix resin, stabilization of the radicals by temperature adjustments have been attempted [92, 93]. However, determining the optimum silane condition for a specific system is extremely difficult because silane performance is affected by several factors, including surface energy, acid-base interaction, interpenetrating network formation, and covalent reaction [92, 94, 95].

After seven days of immersion of the KAB in water, the silane coupling ratio reduced to 68.4%, suggesting that 9.8% of the silane coupling layer was hydrolyzed. The alkoxy group of silane changed to a silanol group by activation, which generates a covalent bond or hydrogen bond on the surface of inorganic fillers [24]. The covalent bonds between the alkoxy group and inorganic filler provide stabilization at the organic/inorganic interface [95]. However, interfacial hydrogen bonds under humid environments break [94]. Furthermore, the organofunctional group of silane is bonded with the matrix resin, generating ester bonds, which are hydrolyzable [30]. To overcome this aspect, hydrolytic durable coupling agents have been developed by modifying the siloxane structure into hydrophobic polyfluoroalkyltrimethoxysilanes [96] or by elongating the linker group structure of the silane agent [97].

After seven days of immersion in water, the elastic modulus of the bulk block of KAB decreased from 8.2 GPa to 6.9 GPa. The elastic modulus of the matrix resin decreased from 3.0 GPa to 2.7 GPa. The coupling ratio decreased from 78.2% to 68.4%. The reduction of the chemico–mechanical values for each component showed similar tendency as the bulk block. However, after seven days, the overall mechanical properties may reduce even non-linearly [98]. Therefore, long-term change of the silane coupling ratio should be further investigated.

VI. Conclusion

In this study, water absorption of the CAD/CAM resin composites resulted in reduction of the elastic modulus of the matrix resin and hydrolysis of the silane coupling layer. Regarding the matrix resin, degradation in the elastic modulus was estimated during water immersion using *in vitro* and *in silico* three-point bending tests. Furthermore, hydrolysis of the silane coupling layer during water immersion was verified as the main cause for reduction of the elastic modulus of CAD/CAM resin composites. The *in vitro* and *in silico* approaches established in this study were able to predict the silane coupling ratio of CAD/CAM resin composites, clearly demonstrating its decrease by water absorption.

VII. Acknowledgement

I would like to express my deepest appreciation to Professor Satoshi Imazato, Osaka University Graduate School of Dentistry, Department of Biomaterials Science, who provided insight and expertise that greatly supported the research. I cannot express enough thanks to Associate Professor Satoshi Yamaguchi. His immense knowledge and experience encouraged me throughout my academic research and daily life.

I would also like to extend my sincere thanks to Professor Keisuke Ohta, Kurume University School of Medicine, Department of Anatomy, who cooperated actively in my use of cutting-edge imaging technology including cryo-EM. I am also very grateful to Associate Professor Hiroshisa Yamada, National Institute of Technology, Nara College for advice and support regarding analytic chemistry methods. Furthermore, I would like to thank my colleagues, especially Dr. Kana Kashima and Dr. Akiko Ichikawa, for their collaborative efforts during the research.

Finally, I would like to express my gratitude to my parents and my wife, Akiko Yoritsune. I would not have been able to complete my study without their tremendous understanding and encouragement over the past few years.

VIII. References

[1] Miyazaki T, Hotta Y, Kunii J, Kuriyama S, Tamaki Y. A review of dental CAD/CAM: current status and future perspectives from 20 years of experience. Dent Mater J 2009;28:44-56.

[2] Davidowitz G, Kotick PG. The use of CAD/CAM in dentistry. Dent Clin North Am 2011;55:559-70.

[3] van Noort R. The future of dental devices is digital. Dent Mater 2012;28:3-12.

[4] Duret F, Blouin JL, Duret B. CAD-CAM in dentistry. J Am Dent Assoc 1988;117:715-20.

[5] Duret F, Preston JD. CAD/CAM imaging in dentistry. Curr Opin Dent 1991;1:150-4.

[6] Attia A, Abdelaziz KM, Freitag S, Kern M. Fracture load of composite resin and feldspathic all-ceramic CAD/CAM crowns. J Prosthet Dent 2006;95:117-23.

[7] Alamoush RA, Silikas N. Effect of the composition of CAD/CAM composite blocks on mechanical properties. Biomed Res Int 2018;2018:1-8.

[8] Awad D, Stawarczyk B, Liebermann A, Ilie N. Translucency of esthetic dental restorative CAD/CAM materials and composite resins with respect to thickness

and surface roughness. J Prosthet Dent 2015;113:534-40.

[9] Lauvahutanon S, Takahashi H, Shiozawa M, Iwasaki N, Asakawa Y, Oki M, Finger WJ, Arksornnukit M. Mechanical properties of composite resin blocks for CAD/CAM. Dent Mater J 2014;33:705-10.

[10] Chavali R, Nejat AH, Lawson NC. Machinability of CAD-CAM materials. J Prosthet Dent 2017;118:194-9.

[11] Ferracane JL. Resin composite--state of the art. Dent Mater 2011;27:29-38.

[12] Pratap B, Gupta RK, Bhardwaj B, Nag M. Resin based restorative dental materials: characteristics and future perspectives. Jpn Dent Sci Rev 2019;55:126-38.

[13] Ruse ND, Sadoun MJ. Resin-composite blocks for dental CAD/CAM applications. J Dent Res 2014;93:1232-4.

[14] Piconi C, Maccauro G. Zirconia as a ceramic biomaterial. Biomaterials 1999;20:1-25.

[15] Goumans TP, Wander A, Brown WA, Catlow CR. Structure and stability of the (001) α-quartz surface. Phys Chem Chem Phys 2007;9:2146-52.

[16] Wolanov Y, Shurki A, Prikhodchenko PV, Tripoľskaya TA, Novotortsev VM, Pedahzur R, Lev O. Aqueous stability of alumina and silica perhydrate

hydrogels: experiments and computations. Dalton Trans 2014;43:16614-25.

[17] Endo T, Finger WJ, Kanehira M, Utterodt A, Komatsu M. Surface texture and roughness of polished nanofill and nanohybrid resin composites. Dent Mater J 2010;29:213-23.

[18] Mitra SB, Wu D, Holmes BN. An application of nanotechnology in advanced dental materials. J Am Dent Assoc 2003;134:1382-90.

[19] Satterthwaite JD, Vogel K, Watts DC. Effect of resin-composite filler particle size and shape on shrinkage-strain. Dent Mater 2009;25:1612-5.

[20] Lu H, Lee YK, Oguri M, Powers JM. Properties of a dental resin composite with a spherical inorganic filler. Oper Dent 2006;31:734-40.

[21] Okada K, Kameya T, Ishino H, Hayakawa T. A novel technique for preparing dental CAD/CAM composite resin blocks using the filler press and monomer infiltration method. Dent Mater J 2014;33:203-9.

[22] Söderholm KJ, Shang SW. Molecular orientation of silane at the surface of colloidal silica. J Dent Res 1993;72:1050-4.

[23] Chen JH, Matsumura H, Atsuta M. Effect of etchant, etching period, and silane priming on bond strength to porcelain of composite resin. Oper Dent 1998;23:250-7.

[24] Nihei T. Dental applications for silane coupling agents. J Oral Sci 2016;58:151-5.

[25] Hooshmand T, Keshvad A, van Noort R. XPS analysis of silane films on the surface of a dental ceramic. J Adhes Sci Technol 2009;23:1085-95.

[26] Pantano CG, Wittberg TN. XPS analysis of silane coupling agents and silane-treated E-glass fibers. Surf Interface Anal 1990;15:498-501.

[27] Nguyen JF, Migonney V, Ruse ND, Sadoun M. Resin composite blocks via high-pressure high-temperature polymerization. Dent Mater 2012;28:529-34.

[28] Khatri CA, Stansbury JW, Schultheisz CR, Antonucci JM. Synthesis, characterization and evaluation of urethane derivatives of Bis-GMA. Dent Mater 2003;19:584-8.

[29] Söderholm KJ, Mariotti A. BIS-GMA--based resins in dentistry: are they safe? J Am Dent Assoc 1999;130:201-9.

[30] Koin PJ, Kilislioglu A, Zhou M, Drummond JL, Hanley L. Analysis of the degradation of a model dental composite. J Dent Res 2008;87:661-5.

[31] Santos C, Clarke RL, Braden M, Guitian F, Davy KW. Water absorption characteristics of dental composites incorporating hydroxyapatite filler. Biomaterials 2002;23:1897-904.

[32] Söderholm KJ, Zigan M, Ragan M, Fischlschweiger W, Bergman M. Hydrolytic degradation of dental composites. J Dent Res 1984;63:1248-54.

[33] Sideridou I, Tserki V, Papanastasiou G. Study of water sorption, solubility and modulus of elasticity of light-cured dimethacrylate-based dental resins. Biomaterials 2003;24:655-65.

[34] Oysaed H, Ruyter IE. Composites for use in posterior teeth: mechanical properties tested under dry and wet conditions. J Biomed Mater Res 1986;20:261-71.

[35] Söderholm KJ, Roberts MJ. Influence of water exposure on the tensile strength of composites. J Dent Res 1990;69:1812-6.

[36] Lene F, Leguillon D. Homogenized constitutive law for a partially cohesive composite material. Int J Solids Struc 1982;18:443-58.

[37] Francfort GA. Homogenization and linear thermoelasticity. SIAM J Math Anal 1983;14:696-708.

[38] Guedes J, Kikuchi N. Preprocessing and postprocessing for materials based on the homogenization method with adaptive finite element methods. Comput Methods in Appl Mech Eng 1990;83:143-98.

[39] Takano N, Zako M, Kubo F, Kimura K. Microstructure-based stress analysis and

evaluation for porous ceramics by homogenization method with digital image-based modeling. Int J Solids Struct 2003;40:1225-42.

[40] Takano N, Fukasawa K, Nishiyabu K. Structural strength prediction for porous titanium based on micro-stress concentration by micro-CT image-based multiscale simulation. Int J Mech Sci 2010;52:229-35.

[41] Peng RD, Zhou HW, Wang HW, Mishnaevsky L. Modeling of nano-reinforced polymer composites: Microstructure effect on Young's modulus. Comput Mater Sci 2012;60:19-31.

[42] Mortazavi B, Bardon J, Ahzi S. Interphase effect on the elastic and thermal conductivity response of polymer nanocomposite materials: 3D finite element study. Comput Mater Sci 2013;69:100-6.

[43] Pontefisso A, Zappalorto M, Quaresimin M. An efficient RVE formulation for the analysis of the elastic properties of spherical nanoparticle reinforced polymers. Comput Mater Sci 2015;96:319-26.

[44] Bernardo LFA, Amaro APBM, Pinto DG, Lopes SMR. Modeling and simulation techniques for polymer nanoparticle composites – A review. Comput Mater Sci 2016;118:32-46.

[45] Yamaguchi S, Inoue S, Sakai T, Abe T, Kitagawa H, Imazato S. Multi-scale

analysis of the effect of nano-filler particle diameter on the physical properties of CAD/CAM composite resin blocks. Comput Methods Biomech Biomed Engin 2017;20:714-9.

[46] Gulec L, Ulusoy N. Effect of endocrown restorations with different CAD/CAM materials: 3D finite element and weibull analyses. Biomed Res Int 2017;2017:1-10.

[47] Stocchero M, Jinno Y, Toia M, Jimbo R, Lee C, Yamaguchi S, Imazato S, Becktor JP. In silico multi-scale analysis of remodeling peri-implant cortical bone: a comparison of two types of bone structures following an undersized and non-undersized technique. J Mech Behav Biomed Mater 2020;103:103598.

[48] Hollister SJ, Kikuchi N. Homogenization theory and digital imaging: a basis for studying the mechanics and design principles of bone tissue. Biotechnol Bioeng 1994;43:586-96.

[49] Hollister SJ, Brennan J, Kikuchi N. A homogenization sampling procedure for calculating trabecular bone effective stiffness and tissue level stress. J Biomech 1994;27:433-44.

[50] Nagai K, Sato Y, Ueda T. Mesoscopic simulation of failure of mortar and concrete by 2D RBSM. J Adv Concr Technol 2004;2:359-74.

[51] Terada K, Miura T, Kikuchi N. Digital image-based modeling applied to the homogenization analysis of composite materials. Comput Mech 1997;20:331-46.

[52] ISO4049:2019. Dentistry - Polymer-based restorative materials. International Organization for Standardization 2019.

[53] Carlotti G, Doucet L, Dupeux M. Elastic properties of silicon dioxide films deposited by chemical vapour deposition from tetraethylorthosilicate. Thin Solid Films 1997;296:102-5.

[54] Dang TA, Gnanasekaran R, Deppe DD. Quantification of surface hydroxides using chemical labeling and XPS. Surf Interface Anal 1992;18:141-6.

[55] McCafferty E, Wightman JP. Determination of the concentration of surface hydroxyl groups on metal oxide films by a quantitative XPS method. Surf Interface Anal 1998;26:549-64.

[56] Yoshida Y, Shirai K, Nakayama Y, Itoh M, Okazaki M, Shintani H, Inoue S, Lambrechts P, Vanherle G, Van Meerbeek B. Improved filler-matrix coupling in resin composites. J Dent Res 2002;81:270-3.

[57] Matinlinna JP, Lung CYK, Tsoi JKH. Silane adhesion mechanism in dental applications and surface treatments: A review. Dent Mater 2018;34:13-28.

[58] Wang BG, Yamaguchi T, Nakao SI. Solvent diffusion in amorphous glassy

polymers. J Polym Sci B Polym Phys 2000;38:846-56.

[59] Patil R, Mark J, Apostolov A, Vassileva E, Fakirov S. Crystallization of water in some crosslinked gelatins. Eur Polym J 2000;36:1055-61.

[60] Ping Z, Nguyen Q, Chen S, Zhou J, Ding Y. States of water in different hydrophilic polymers-DSC and FTIR studies. Polymer 2001;42:8461-7.

[61] Sideridou ID, Achilias DS, Karabela MM. Sorption kinetics of ethanol/water solution by dimethacrylate-based dental resins and resin composites. J Biomed Mater Res Part B Appl Biomater 2007;81:207-18.

[62] Sideridou ID, Karabela MM. Sorption of water, ethanol or ethanol/water solutions by light-cured dental dimethacrylate resins. Dent Mater 2011;27:1003-10.

[63] Ferracane JL. Hygroscopic and hydrolytic effects in dental polymer networks. Dent Mater 2006;22:211-22.

[64] Debnath S, Wunder SL, McCool JI, Baran GR. Silane treatment effects on glass/resin interfacial shear strengths. Dent Mater 2003;19:441-8.

[65] Brochier Salon M-C, Bayle P-A, Abdelmouleh M, Boufi S, Belgacem MN. Kinetics of hydrolysis and self condensation reactions of silanes by NMR spectroscopy. Colloid Surf A Physicochem Eng Asp 2008;312:83-91.

[66] Arksornnukit M, Takahashi H, Nishiyama N. Effects of silane coupling agent amount on mechanical properties and hydrolytic durability of composite resin after hot water storage. Dent Mater J 2004;23:31-6.

[67] Randolph LD, Palin WM, Leloup G, Leprince JG. Filler characteristics of modern dental resin composites and their influence on physico-mechanical properties. Dent Mater 2016;32:1586-99.

[68] Nathawat R, Kumar A, Acharya NK, Vijay YK. XPS and AFM surface study of PMMA irradiated by electron beam. Surf Coat Tech 2009;203:2600-4.

[69] Jandt KD. Atomic force microscopy of biomaterials surfaces and interfaces. Surf Sci 2001;491:303-32.

[70] Çağlayan M. Nanomechanical characterization of flowable dental restorative nanocomposite resins using AFM. Polymer Plast Tech Eng 2017;56:1813-21.

[71] Mate CM, McClelland GM, Erlandsson R, Chiang S. Atomic-scale friction of a tungsten tip on a graphite surface. Phys Rev Lett 1987;59:1942-5.

[72] Wu Y, Fang Y, Fan Z, Wang C, Liu C. An automated vertical drift correction algorithm for AFM images based on morphology prediction. Micron 2021;140:102950.

[73] Dupraz AMP, de Wijn JR, v.d. Meer SAT, de Groot K. Characterization of

silane-treated hydroxyapatite powders for use as filler in biodegradable composites. J Biomed Mater Res 1996;30:231-8.

[74] Dietrich PM, Streeck C, Glamsch S, Ehlert C, Lippitz A, Nutsch A, Kulak N, Beckhoff B, Unger WES. Quantification of silane molecules on oxidized silicon: Are there options for a traceable and absolute determination? Anal Chem 2015;87:10117-24.

[75] Rosentritt M, Preis V, Behr M, Hahnel S. Influence of preparation, fitting, and cementation on the vitro performance and fracture resistance of CAD/CAM crowns. J Dent 2017;65:70-5.

[76] Kucukelbir A, Sigworth FJ, Tagare HD. Quantifying the local resolution of cryo-EM density maps. Nat Methods 2014;11:63-5.

[77] Kim S, Jeong Park M, Balsara NP, Liu G, Minor AM. Minimization of focused ion beam damage in nanostructured polymer thin films. Ultramicroscopy 2011;111:191-9.

[78] Lang B, Jaarda M, WANG R. Filler particle size and composite resin classification systems. J Oral Rehabil 1992;19:569-84.

[79] Rastelli AN, Jacomassi DP, Faloni APS, Queiroz TP, Rojas SS, Bernardi MIB, Bagnato VS, Hernandes AC. The filler content of the dental composite resins

and their influence on different properties. Microsc Res Tech 2012;75:758-65.

[80] Miyasaka T. Effect of shape and size of silanated fillers on mechanical properties of experimental photo cure composite resins. Dent Mater J 1996;15:98-110.

[81] Asano R, Otake S, Nozaki K, Yoshida K, Miura H. Effect of elapsed time after air abrasion on bond strength of luting agent to CAD/CAM resin blocks. J Oral Sci 2019;61:459-67.

[82] Kimura S, Shimizu T, Fujii B. Influence of dentin on bonding of composite resin. Dent Mater J 1985;4:68-80.

[83] Sakai T, Li H, Abe T, Yamaguchi S, Imazato S. Multi-scale analysis of the influence of filler shapes on the mechanical performance of resin composites using high resolution nano-CT images. Dent Mater 2020;37:168-74.

[84] Lung C, Matinlinna J. Silanes for adhesion promotion and surface modification. (Book) Nova Science Pub Inc, Hauppauge, 2013; 87-109.

[85] Chambers RC, Jones Jr WE, Haruvy Y, Webber SE, Fox MA. Influence of steric effects on the kinetics of ethyltrimethoxysilane hydrolysis in a fast sol-gel system. Chem Mater 1993;5:1481-6.

[86] Brinker CJ. Hydrolysis and condensation of silicates: effects on structure. J Non

Cryst Solids 1988;100:31-50.

[87] Jiang H, Zheng Z, Li Z, Wang X. Effects of temperature and solvent on the hydrolysis of alkoxysilane under alkaline conditions. Ind Eng Chem Res 2006;45:8617-22.

[88] Jiang H, Zheng Z, Wang X. Kinetic study of methyltriethoxysilane (MTES) hydrolysis by FTIR spectroscopy under different temperatures and solvents. Vib Spectrosc 2008;46:1-7.

[89] Lung CY, Matinlinna JP. Resin bonding to silicatized zirconia with two isocyanatosilanes and a cross-linking silane. Part I: experimental. Silicon 2010;2:153-61.

[90] Matinlinna JP, Vallittu PK. Silane based concepts on bonding resin composite to metals. J Contemp Dent Pract 2007;8:1-8.

[91] Su Y, Zhou Y, Huang W, Gu Z. Study on reaction kinetics between silica glasses and hydrofluoric acid. J Chin Ceram Soc 2004;32:287-93.

[92] Wang D, Szillat F, Fouassier JP, Lalevée J. Remarkable versatility of silane/Iodonium salt as redox free radical, cationic, and photopolymerization initiators. Macromolecules 2019;52:5638-45.

[93] Burtscher P. Stability of radicals in cured composite materials. Dent Mater

1993;9:218-21.

[94] Choi S, Maul S, Stewart A, Hamilton H, P. Douglas E. Effect of silane coupling agent on the durability of epoxy adhesion for structural strengthening applications. Polym Eng Sci 2013;53:283-94.

[95] Witucki GL. A silane primer: chemistry and applications of alkoxy silanes. J Coat Technol 1993;65:57-8.

[96] Nihei T, Kurata S, Kondo Y, Umemoto K, Yoshino N, Teranaka T. Enhanced hydrolytic stability of dental composites by use of fluoroalkyltrimethoxysilanes. J Dent Res 2002;81:482-6.

[97] Nishiyama N, Ishizaki T, Horie K, Tomari M, Someya M. Novel polyfunctional silanes for improved hydrolytic stability at the polymer-silica interface. J Biomed Mater Res 1991;25:213-21.

[98] Arikawa H, Kuwahata H, Seki H. Deterioration of mechanical properties of composite resins. Dent Mater J 1995;14:78-83.

IX. Tables and Figures

Table 1. Compositions of the materials used

Materials (Manufacturer)	Code	Monomer	Filler	Filler Content (wt%)
Katana Avencia P Block (Kuraray Noritake Dental)	KAP	UDMA‡, TEGDMA‡‡	SiO_2 (40 nm)* Al_2O_3 (20 nm)	82
Experimental Matrix Block	EMB	UDMA‡, TEGDMA‡‡	-	-

‡ UDMA: urethane dimethacrylate

‡‡ TEGDMA: triethylene glycol dimethacrylate

*average diameter

Table 2. Properties of the KAP model for *in silico* homogenization analysis

Filler size	38.6 nm
Elastic modulus of filler	70 GPa
Filler volume	61%
Silane coupling layer thickness	2 nm

Table 3. Composition of KAB

Material (Manufacturer)	**Code**	**Monomer**	**Filler**	**Filler content (vol%)**
Katana Avencia Block (Kuraray Noritake Dental)	KAB	UDMA‡, TEGDMA‡‡	SiO_2 (40 nm)* Al_2O_3 (20 nm)	55

‡ UDMA: urethane dimethacrylate

‡‡ TEGDMA: triethylene glycol dimethacrylate

*average diameter

Table 4. Material properties of *in silico* homogenization model

	Elastic modulus (GPa)	**Volume ratio (%)**
Filler	72	55.16
Matrix	2	44.84

Table 5. Prepared silane coupling ratio

Silane coupling ratio (%)	75.5	81.7	87.9	91.7	94.4	98.1	100
Uncoupled ratio (%)	24.5	18.3	12.1	8.3	5.6	1.9	0

Table 6. Elastic modulus and coupling ratio

Coupling ratio (%)	75.5	81.7	87.92	91.67	94.35	98.1	100
Elastic modulus (GPa)	9.84	9.99	10.08	10.22	10.47	11.18	11.82

Table 7. Elastic moduli (GPa) of KAB and EMB before and after immersion.

	Before immersion	**After immersion**
KAB	8.2	6.9
EMB	3	2.7

Table 8. Coupling ratios and corresponding elastic moduli of the silane coupling layer

Coupling ratio (%)	100	95	90	85	80	75	70	65	60	55	50
Elastic modulus (GPa)	2.00	1.74	1.53	1.37	1.22	1.10	1.00	0.88	0.78	0.69	0.60

Table 9. Prediction of the coupling ratio

	EM_{matrix} (GPa)	EM_{filler} (GPa)	EM_{silane} (GPa)	EM_{model} (GPa)	Coupling ratio (%)
Before immersion	3	72	1.16 ± 0.05	8.19 ± 0.11	78.2 ± 1.64
After immersion	2.7	72	0.92 ± 0.04	6.89 ± 0.15	68.4 ± 0.89

(n = 5)

Figure 1. Experimental block (EMB) made only of resin matrix.
The size of the block is 18 × 15 × 15 mm.

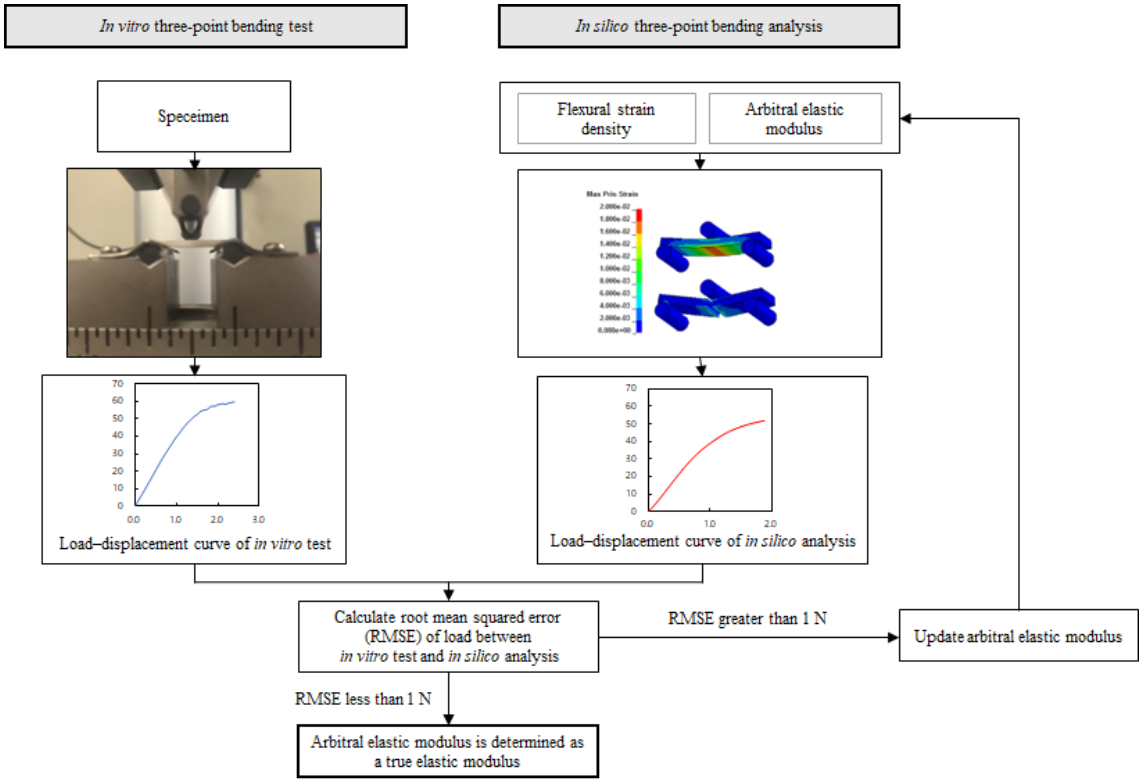

Figure 2. Scheme for determining the true elastic modulus.

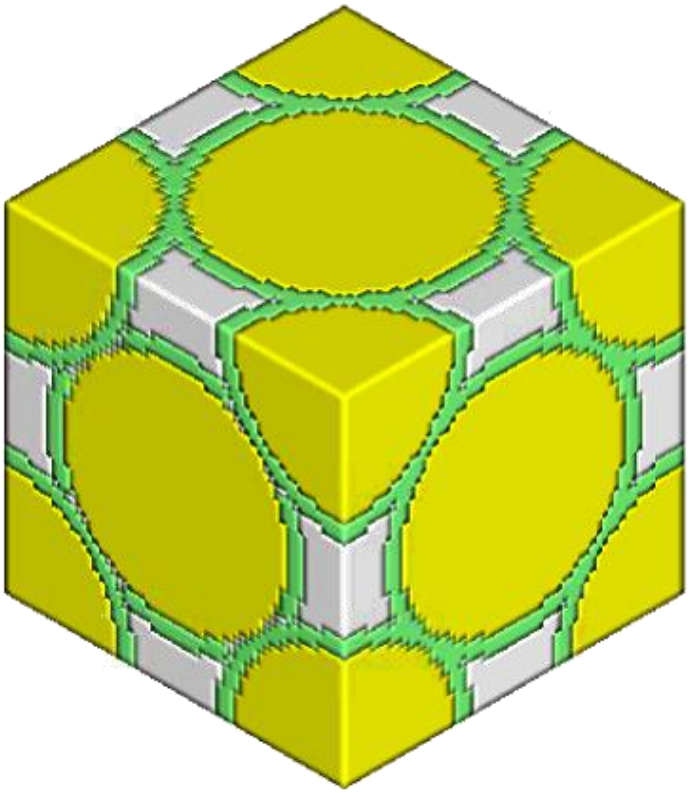

Figure 3. KAP model for the *in silico* homogenization analysis.
The size of the model is 80 × 80 × 80 nm.

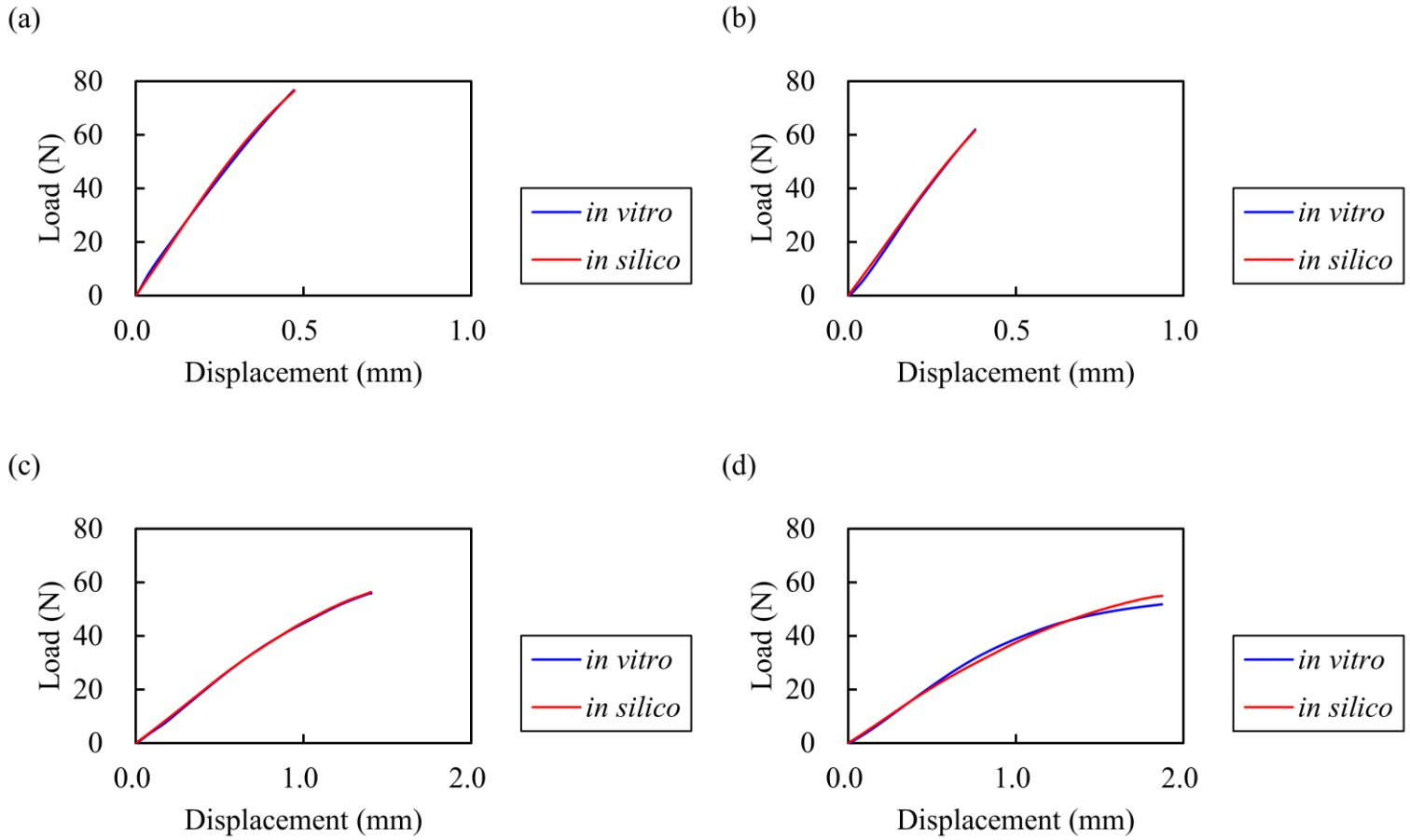

Figure 4. Load–displacement curves of KAP and EMB:
(a) KAP before immersion, (b) KAP after immersion, (c) EMB before immersion, and (d) EMB after immersion.

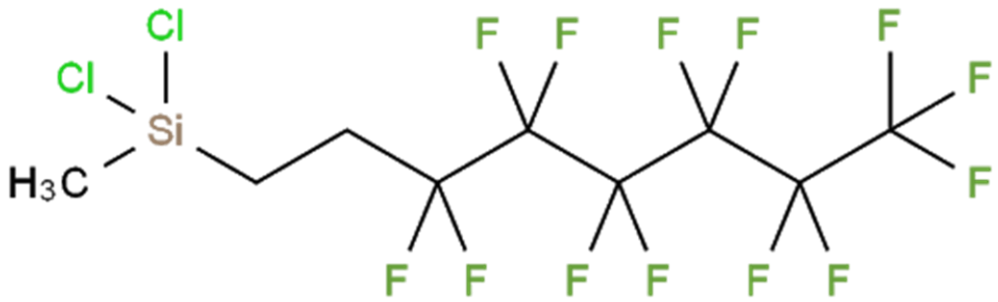

Figure 5. Chemical structure of 1H-1H-2H-2H-perfluorooctylmethyldichlorosilane.

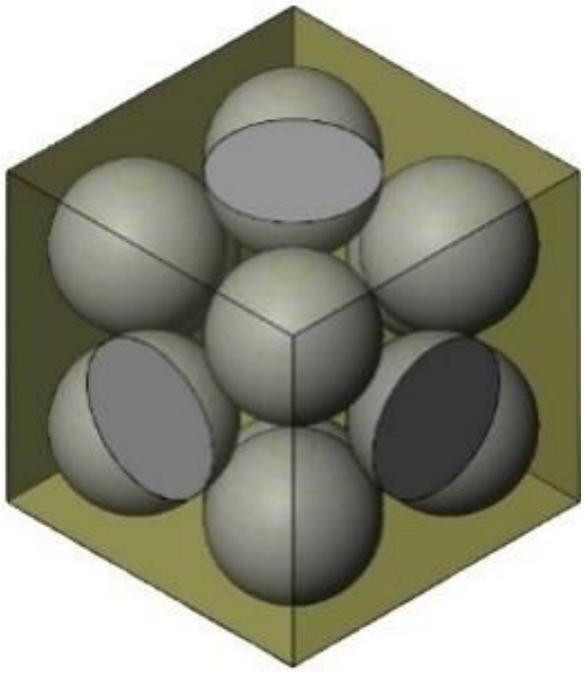

Figure 6. Nano-scale model for the *in silico* homogenization analysis.
The size of the model is 90 × 90 × 90 nm.

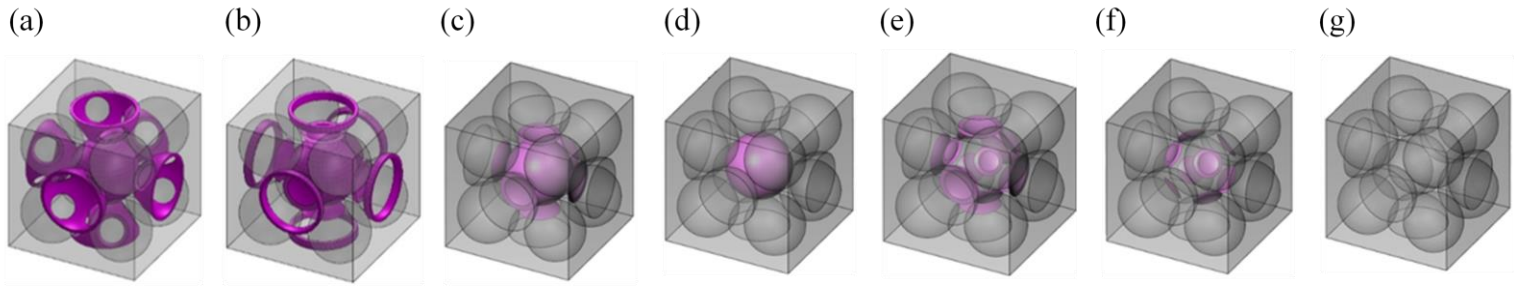

Figure 7. Nano-scale models combined with silane coupling layers of various coupling ratios.
The coupling ratios are (a) 75.5%, (b) 81.7%, (c) 87.9%, (d) 91.7%, (e) 94.4%, (f) 98.1%, and (g) 100%.

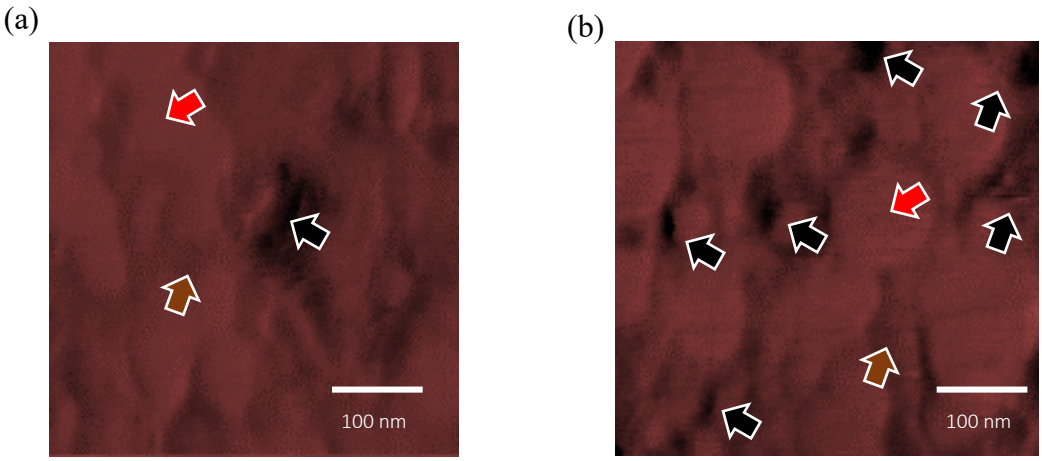

Figure 8. SPM images of KAB (a) before immersion and (b) after immersion.
Red arrows indicate fillers, brown arrows indicate the matrix and silane coupling layer, and black arrows indicate the degraded area.

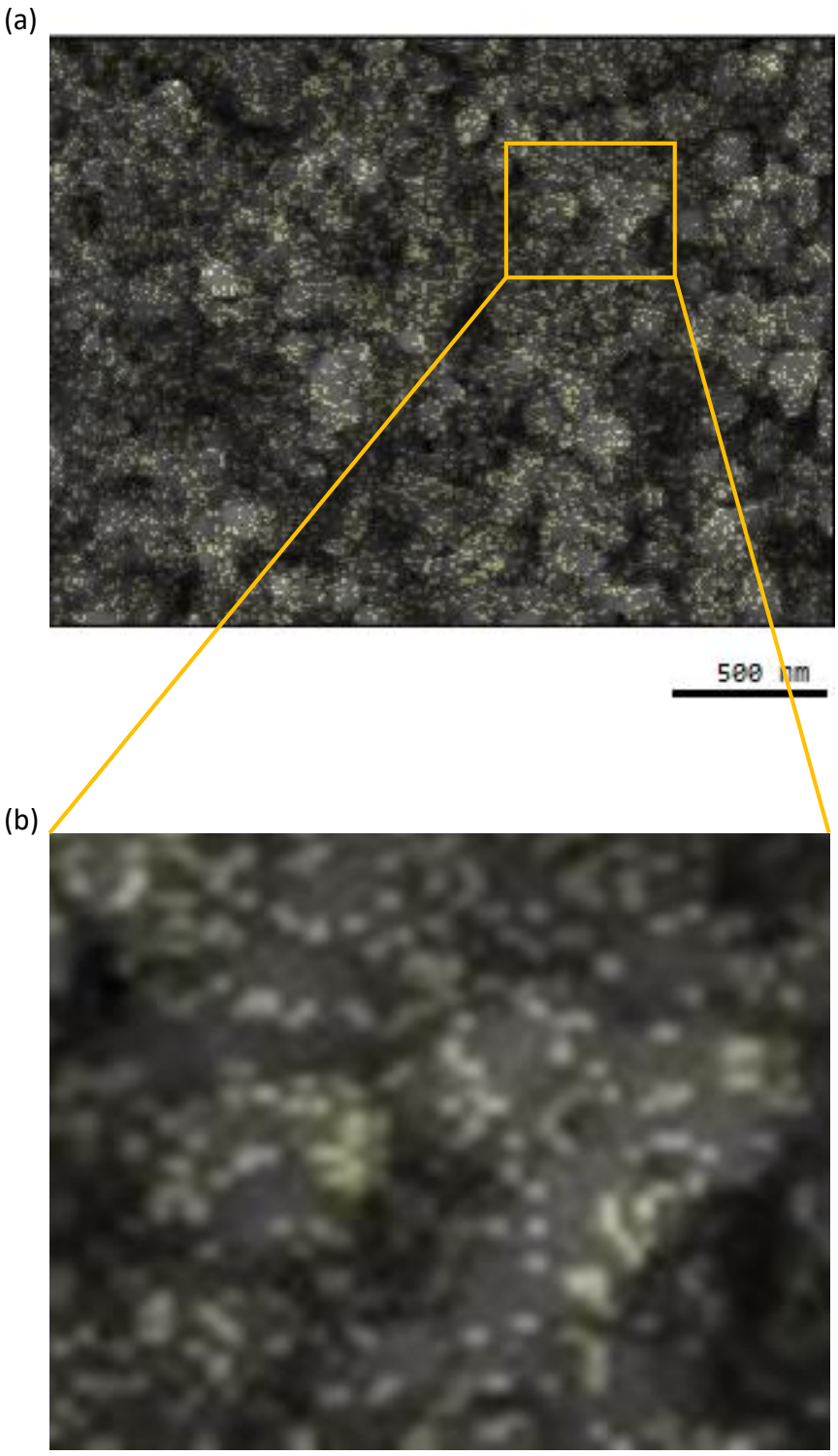

Figure 9. (a) EDX image of fluoride-labeled KAB specimen and (b) 5× magnified image of the square area in (a). Pale yellow dots represented the location of fluoride atoms.

(a)

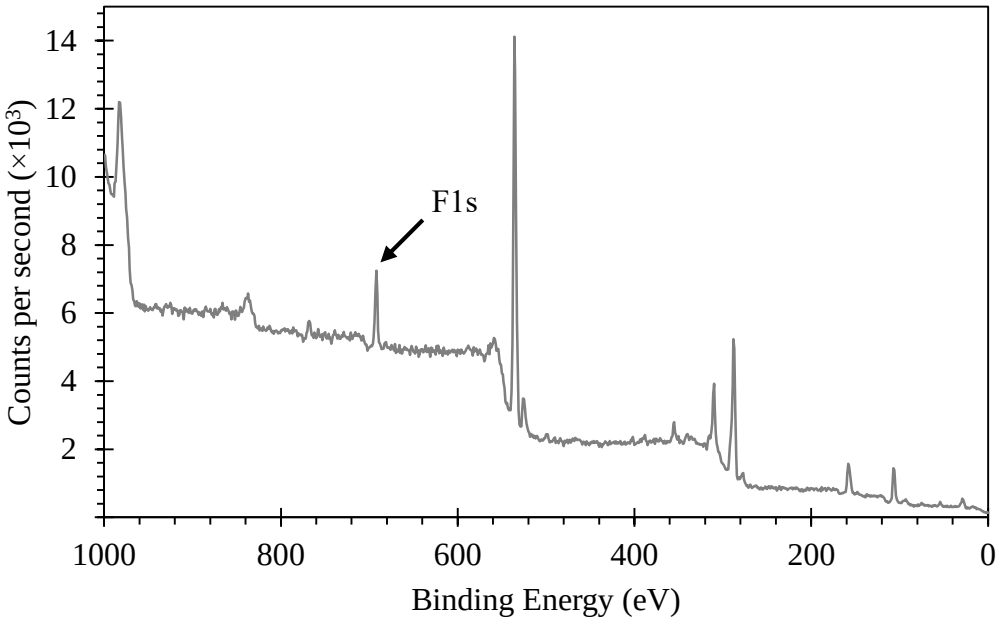

(b)

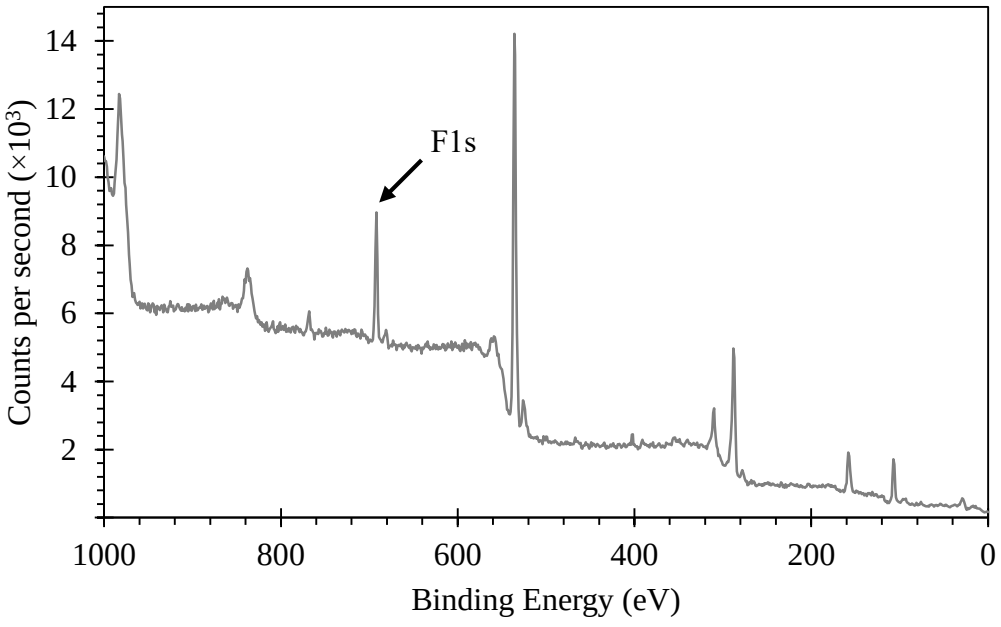

Figure 10. XPS of fluoride-labeled KAB.

(a) before immersion and (b) after immersion.

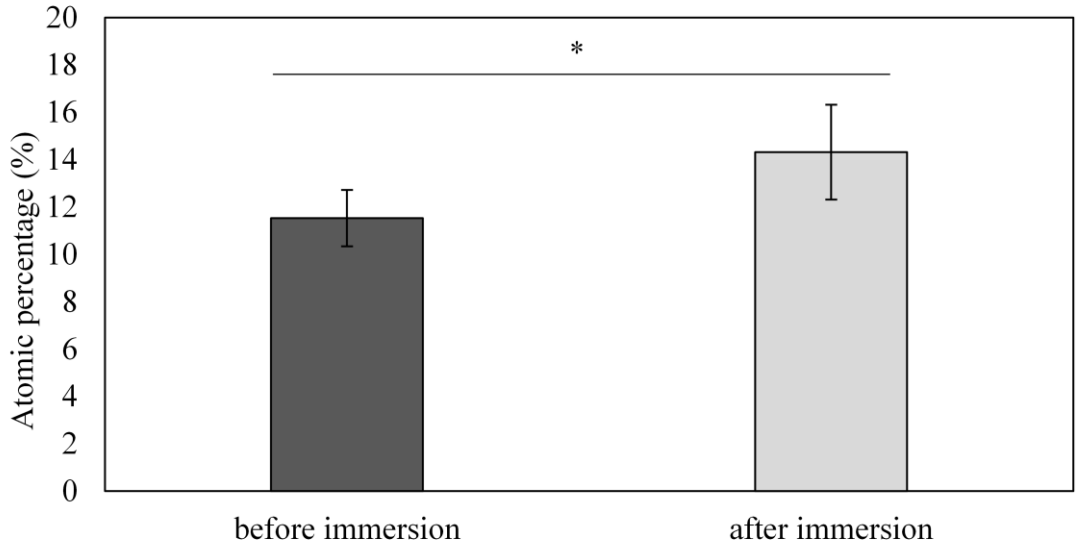

Figure 11. Atomic percentage of F1s on fluoride-labeled KAB.
(Student's *t*-test, $n = 5$, $*p < 0.05$).

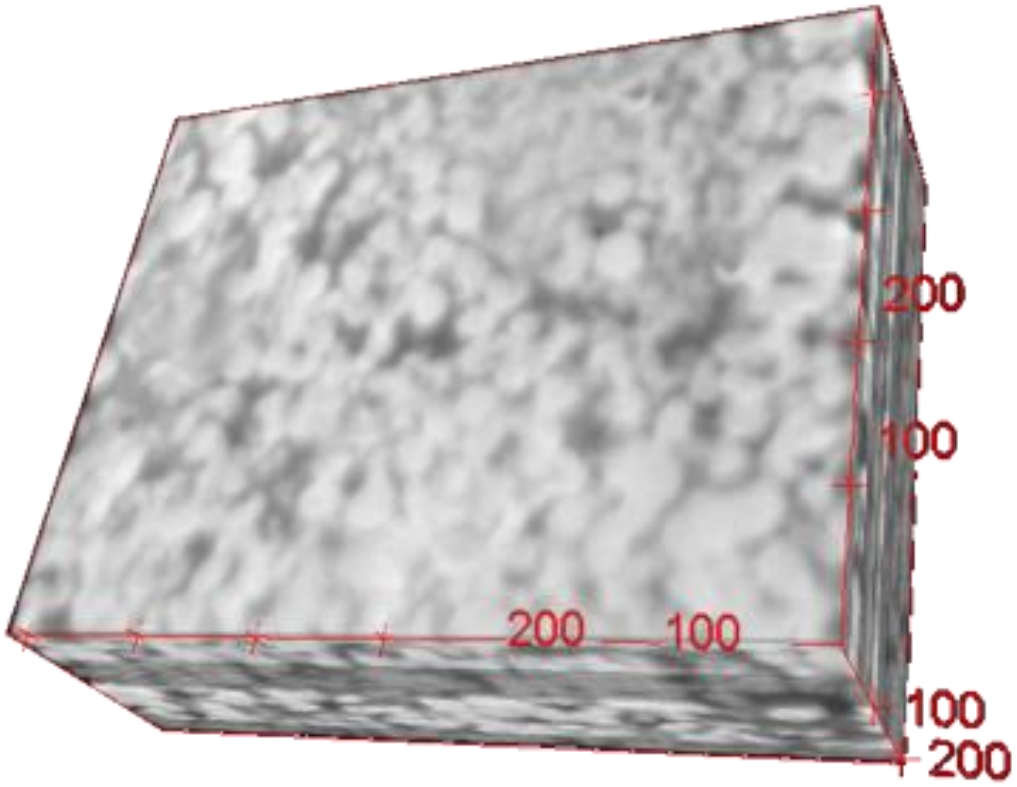

Figure 12. Image stack of cryo-electron microscopy.
The red number indicates voxel coordinates in unit of pixels.

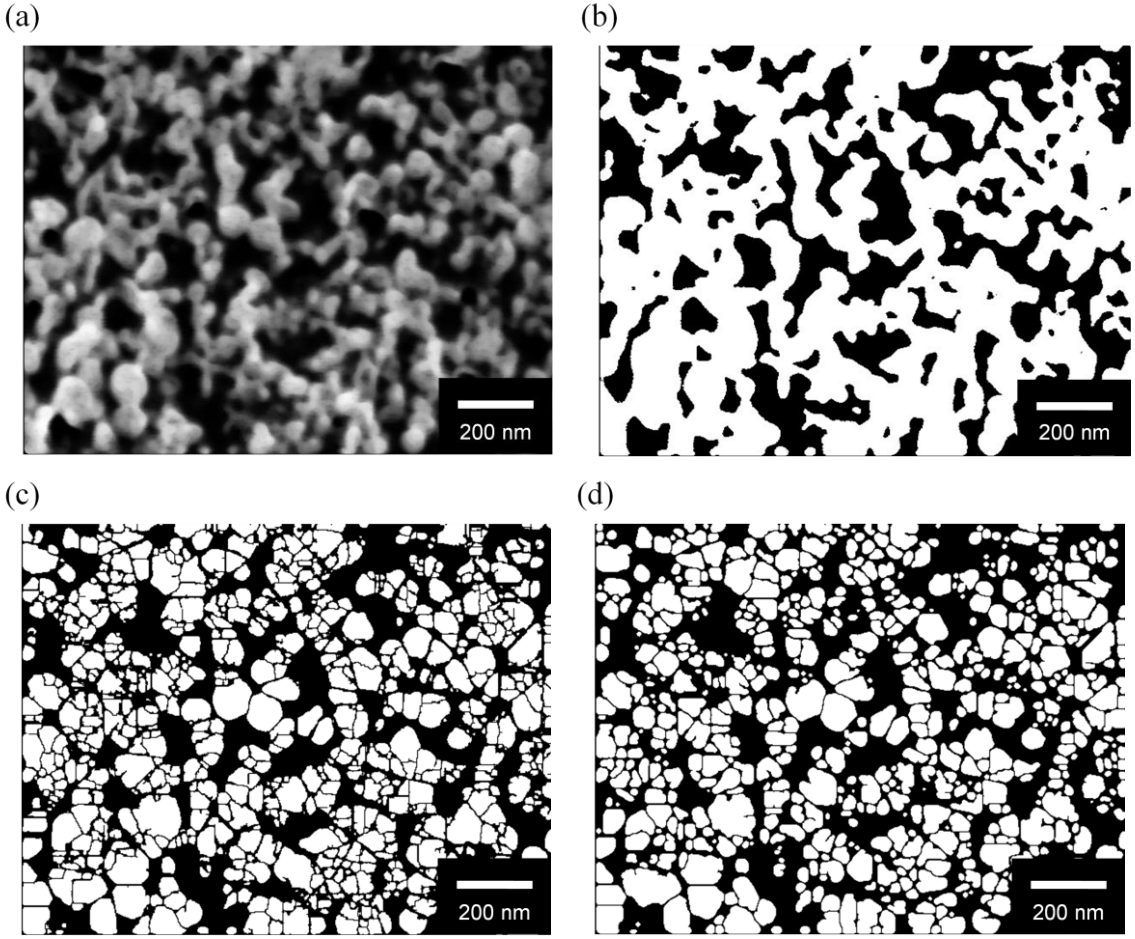

Figure 13. Image processing.

(a) After adjustment of the contrast and brightness, (b) binarization by threshold apply, (c) segmentation, and (d) edge rounding.

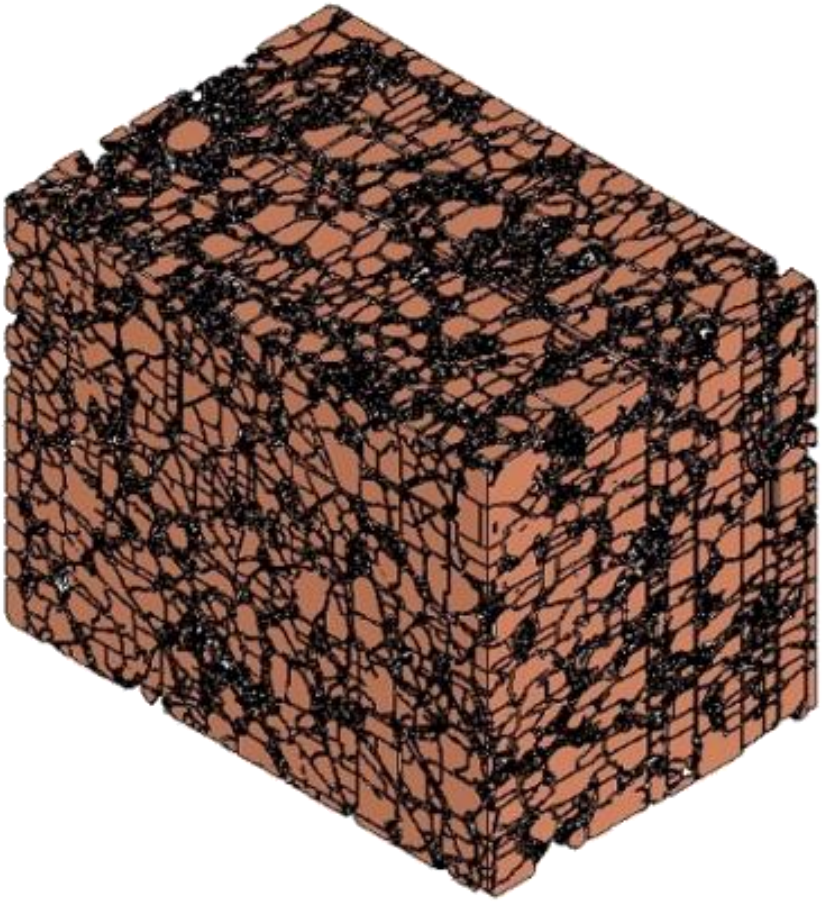

Figure 14. Three dimensional KAB model.

The size of the model is 1.8 × 1.4 × 1.2 μm.

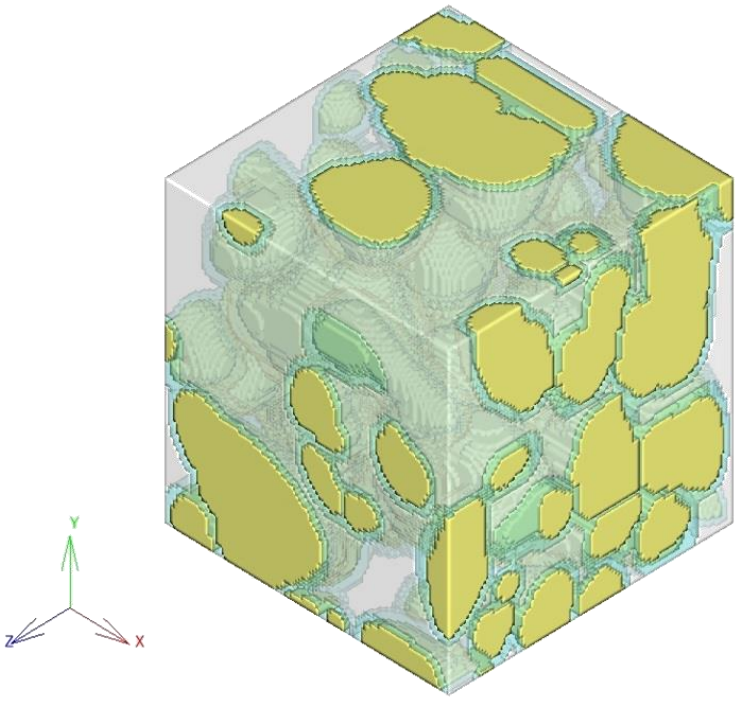

Figure 15. 100-nm cubic submodel of KAB.

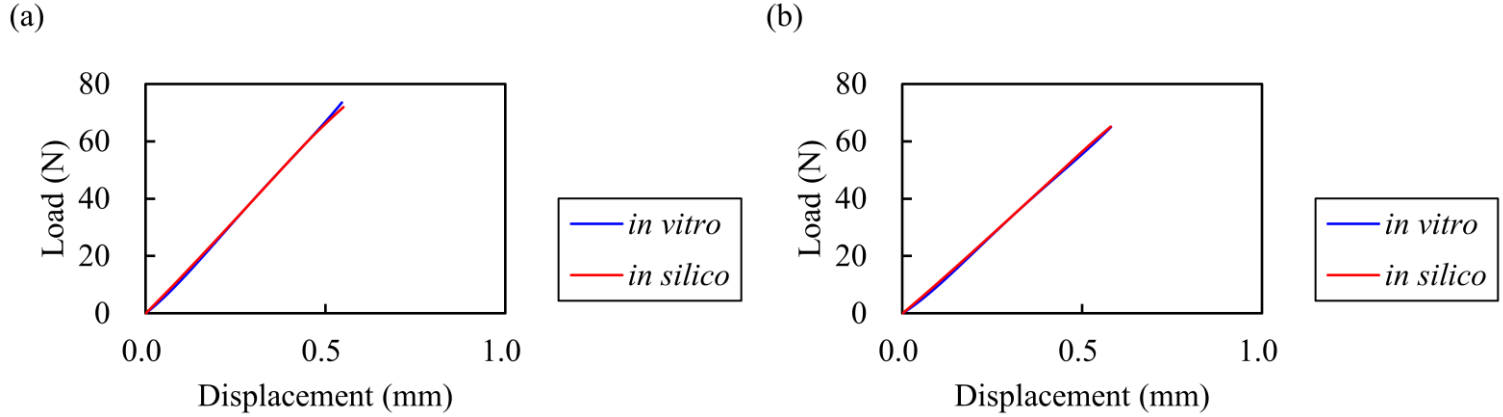

Figure 16. Load–displacement curves of KAB (a) before immersion and (b) after immersion.